2001

Study of 5 and 10 mm thick CZT strip detectors

John R. Macri
University of New Hampshire - Main Campus, John.Macri@unh.edu

Pierre C. Dufour
University of Montreal

L A. Hamel
University of Montreal

M Julien
University of Montreal

Mark L. McConnell
University of New Hampshire - Main Campus, mark.mcconnell@unh.edu

See next page for additional authors

Recommended Citation

Authors

John R. Macri, Pierre C. Dufour, L A. Hamel, M Julien, Mark L. McConnell, M McClish, James M. Ryan, and Mark Widholm

Study of 5 and 10 mm Thick CZT Strip Detectors

J. R. Macri[1], P. Dufour[2], L. A. Hamel[2], M. Julien[2],
M. L. McConnell[1], M. McClish[1], J. M. Ryan[1], M. Widholm[1]

[1] Space Science Center, University of New Hampshire, Durham, NH 03824 USA
[2] Department of Physics, University of Montreal, Montreal, H3C 3J7, Canada

Abstract

We report progress in the study of 5 and 10 mm thick CZT strip detectors featuring orthogonal coplanar anode contacts. This novel anode geometry combines the advantages of pixel detectors with those of double-sided strip detectors. Like pixel detectors, these are electron-only devices that perform well as hard x-ray and γ-ray spectrometers and imagers even in the thicker configurations required for reasonable detection efficiency at 1 MeV. Like double-sided strip detectors in an N × N configuration, these detectors require only 2N readout channels to form N^2 "pixels". Unlike double-sided strip detectors, all signal contacts for spectroscopy and 3-d imaging are formed on one detector surface. Polymer flip chip bonding to a ceramic substrate is employed resulting in a rugged and compact detector assembly. Prototype detector modules 5 mm thick have been fabricated and tested. Prototype modules, 10 mm thick, are currently in procurement. Measurements confirm these devices are efficient detectors throughout their volume. Sub-millimeter position resolution and energy resolution (FWHM) better than 3% at 662 keV and 15% at 60 keV throughout the detector volume are demonstrated. Options for processing the signals from the non-collecting anode strip contacts are discussed. Results from tests of one prototype circuit are presented.

We also report on detector simulation studies aimed at defining an optimum geometry for the anode contacts and at determining optimum operating conditions and the requirements of the signal processing electronics.

I. INTRODUCTION

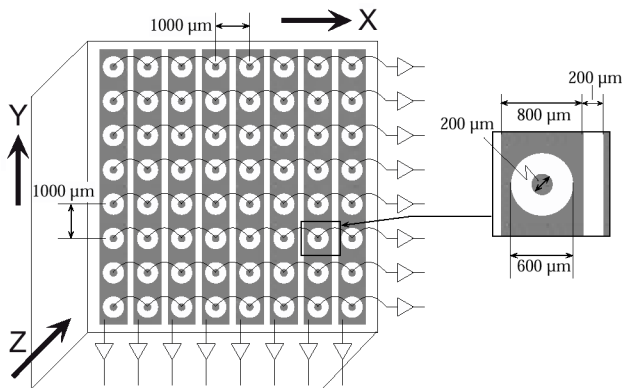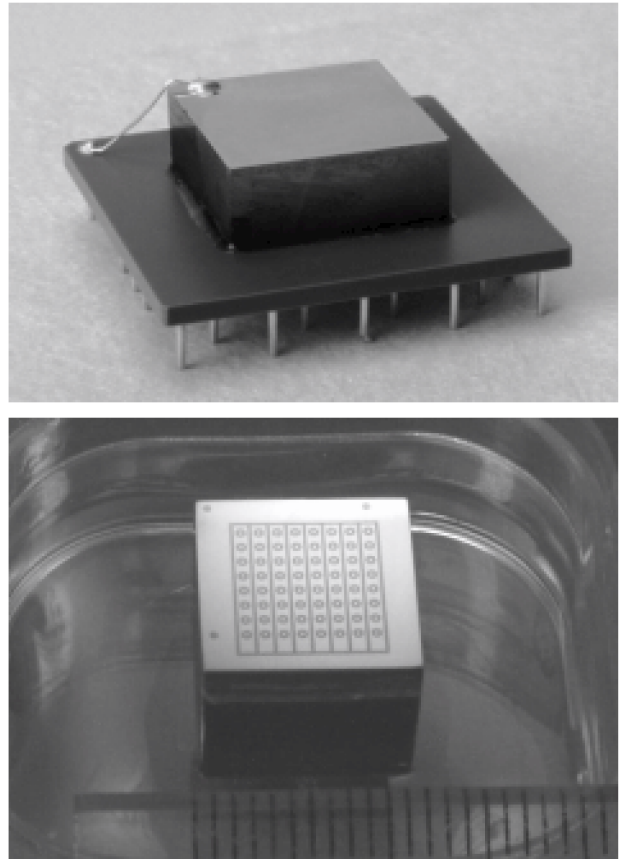Figure 1 illustrates the orthogonal coplanar strip anode

Figure 2. Top: Prototype detector assembly. A 5 mm thick patterned CZT substrate is PFC-bonded to its mating ceramic carrier. Bottom: 10 mm thick patterned CZT substrate. Each mark on scale is 1 mm.

Figure 1. Layout and read out of the orthogonal coplanar anode strip design.

contact pattern with the gold contacts shown in gray. A single cathode contact covers the opposite surface. A signal from each interconnected pixel row provides the energy and Y coordinate. A signal from each orthogonal strip, biased between cathode and pixel row potentials, provides the X and Z coordinates [1]. Figure 2 (top) is a photograph of a 5 mm thick prototype detector. The single cathode contact is seen at the top. Polymer flip chip (PFC) bonding is used to connect the anode contact pads with the ceramic carrier and to form a rugged detector assembly [2]. Figure 2 (bottom) is a photograph of a recently procured patterned 10 mm CZT substrate awaiting detector assembly.

Excellent energy resolution (<1% FWHM at 662 keV, <6% FWHM at 60 keV for a single "pixel") and sub-

millimeter position resolution in each of 3 dimensions was previously reported with the 5 mm thick prototypes [1]. Temperature cycle and vibration tests as well as more than one year of continuous operation in the lab have provided confidence in the ruggedness and stability of the PFC assembly approach. Charge transport and signal generation simulation tools have been developed and validated with laboratory measurements of the prototype detectors.

Having established the feasibility of this approach and developed tools to model and predict detector performance we are now exploring front end electronics options and extending our measurement and simulation effort to thicker detectors. We are working with small area detectors and small numbers of prototypes in order to minimize costs while establishing dependable designs and associated processes. Our goal is to develop mature detector and image plane designs and be ready to employ them in large area detector arrays when large volumes of suitable CZT material with uniform properties become available and affordable.

II. MEASUREMENTS

Setup : All reported measurements were performed using one 5 mm thick prototype detector operating at room temperature. A threshold discriminator was used on each of the 8 pixel row channels. Event acquisition was triggered by a signal above threshold on any pixel row channel. When triggered, pulse height information was acquired for all pixel rows, orthogonal strips, the cathode and guardring. The guard ring potential was set at pixel bias. Amplifiers with 1 μs shaping time were used to process the charge collecting pixel row signals.
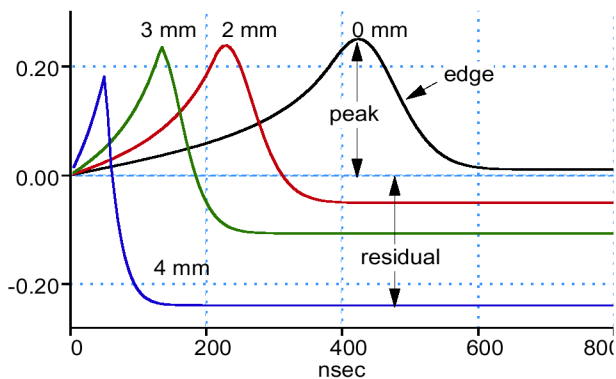

Figure 3. Simulated strip signals at various depths.

By contrast, the orthogonal strip contacts collect no charge but register the motion of electrons as they are collected on the pixels. These are the bipolar signals shown for several interactions depths in Figure 3. The negative edge is a common feature of the strip signal for all regions of the detector. Amplifiers with 200 ns shaping time (integration and differentiation) were used to convert this feature to a pulse height for these measurements.

Efficiency and Uniformity : A detection efficiency measurement was performed using uniform illumination from a ^{57}Co source of known intensity 10 cm from the detector. The measured count rate for the entire 8 x 8 "pixel" region compared very well with calculated expectations. Overall efficiency for detecting and locating events in the 122 keV photopeak was measured to be 99%. Measurement error including geometry, deadtime and source intensity is less than 10%. There are, however, significant non-uniformities. The measured detection efficiency for the eight pixel rows ranges from 66% to 129%. More thorough measurements and analyses are required to understand the sources of the non-uniformity. Measurements are planned with other detector prototypes to assess the importance of material selection, detector processing and fabrication, and variations in contact bias due to leakage.

Spectroscopy : Figure 4 (top) shows the ^{241}Am pulse height spectrum from a single pixel row (8 "pixels"). Figure
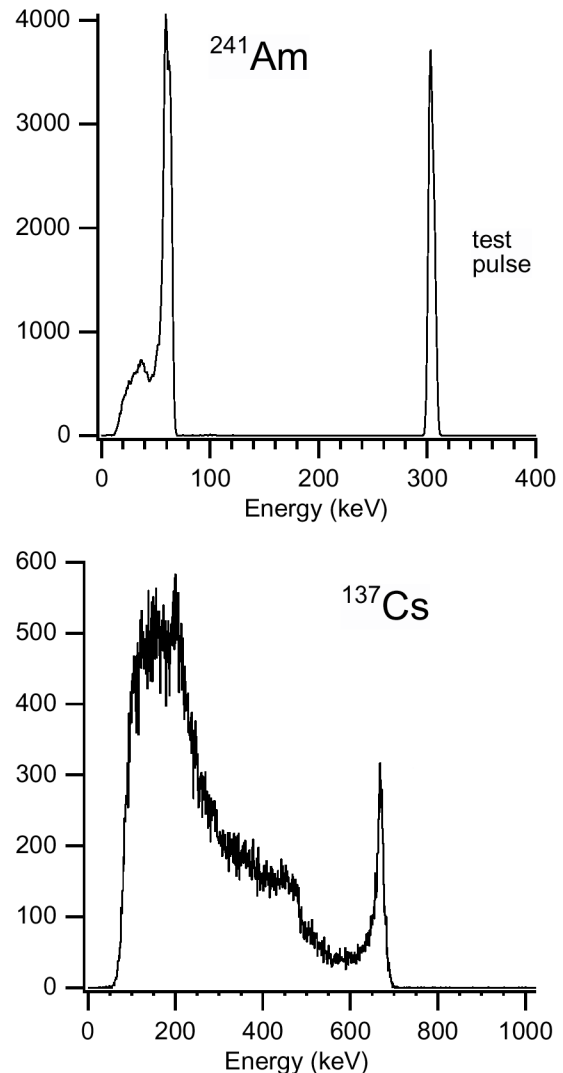

Figure 4. Pixel row spectra. Top: ^{241}Am and test pulse, single pixel row. Bottom: ^{137}Cs, composite of all 8 pixel rows.

4 (bottom) shows a composite spectrum of all eight pixel rows for ^{137}Cs where, for each triggered event, the pulse height of the pixel row having the maximum signal is added with that of its nearest neighbors. Unlike the single "pixel" spectra previously reported [1], all regions of the detector are represented in these spectra. There are no event selections. The measured energy resolution (FWHM) is 15% at 60 keV and 3.0% at 662 keV. The electronic noise with our laboratory setup is 7 keV FWHM for each pixel row channel.

Imaging: Figure 5 illustrates the capability for measuring the X-coordinate of the photon interaction using the orthogonal strip signals. These data were acquired using 122 keV photons from a 200 µm diameter collimated [57]Co source scanned in 100 µm steps along a pixel row axis across three adjacent strips. The left panel is the number of events at the calculated mean value for X vs. the actual X-coordinate of the collimated beam. Note that it tracks well and the spread in calculated X is less than 0.5mm. The right panel shows strip pulse height vs. the source X-coordinate for strip 4. This shows an increase near the edge of the cell and a sharp drop off when the source moves out of the cell. It also shows that the pulse height is better than a factor of two above the noise. The distribution looks narrow enough to be usable for 1mm resolution down to at least 60 keV. Beam spot scans planned using a collimated [241]Am source will confirm this claim. Lower energy thresholds should be achievable with more careful design and layout of the strip signal electronics.
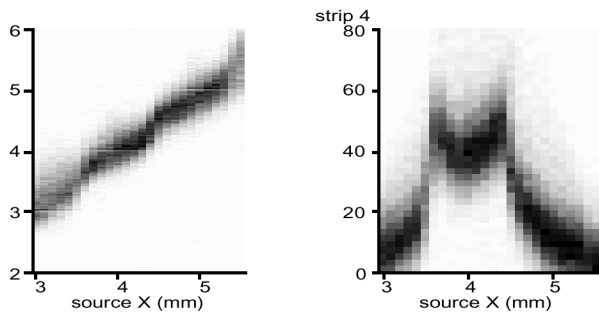

Figure 5. Spot scan in 100 µm steps with 122 keV photons across three strips. Spot size is 200 µm. Left: computed mean value of X-coordinate. Right: pulse height measured for strip 4.

III. ELECTRONICS

Our goal is to develop a compact, low power readout system that processes both the pixel and strip signals of this detector to measure the energy deposit and interaction location in three dimensions. We are presently evaluating options for suitable analog front end circuitry.

Energy and Y-dimension measurement: Processing of the charge collecting pixel row signals for measurement of the energy and Y-dimension is relatively straightforward. We are considering a version of Nova R&D's multi-channel RENA chip for this application [4].

X- and Z-dimension measurements: Of particular interest is the bipolar signal from the strip contacts that collect no charge but register the motion of electrons as they are collected on the pixels (Figure 3). These signals carry the information necessary to determine the X and Z locations of the interaction. Our most recent work is focused on exploring options for processing the strip signals to measure location of the interaction in the X-dimension.

Simulated strip signals were calculated for interactions at points on a 10 x 10 x 15 grid evenly spaced through a 1 x 1 x 5 mm^3 unit cell (one "pixel"). The simulated waveforms were used to investigate how response varies with location. The strip signal is generally bipolar and ranges in amplitude between 25% and 40% of the pixel signal. Its characteristics change significantly depending on the interaction depth.

The goal is to find a simple analog signal processing technique that is sensitive over the entire depth range. Figure 6 shows the relative signal to noise performance expected for a few different shaping options.
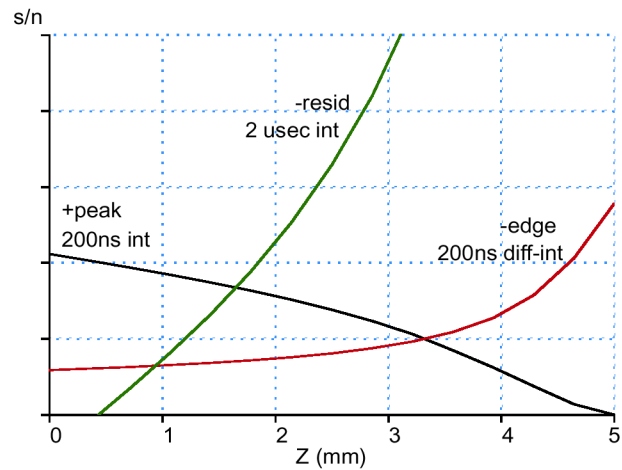

Figure 6. Simulated signal-to-noise ratio (relative units) vs. interaction depth for the X-dimension measurement.

1) Differentiator: One signal characteristic that is relatively uniform over depth is the negative edge (Figure 3). A simple RC differentiator provides shaping that is sensitive to this feature. Differentiating gives a negative peak that is roughly proportional to the peak-to-peak swing. The optimal signal to noise for strip pulses passed though a single stage differentiator-integrator is obtained for time constants in the range of 100 ns to 200 ns. Shorter time constants give a more uniform response over depth but reduce the signal-to-noise ratio. A shaping constant of 200 ns was employed for the measurements shown in Section II.

2) Positive Peak: Although the differentiator-integrator shaping gives fairly uniform response over depth it does not give maximum sensitivity at all depths. The weakest strip pulse comes from interactions near the cathode ($Z=0$) (Figure 3). The differentiator-integrator shaping is sensitive only to the falling edge so it is inherently noisier than looking at the

longer duration peak. Using integrator only shaping and converting the positive peak results in a better signal-to-noise ratio for these weak signals. The amplitude of the positive peak decreases to zero for interactions near the anode so this shaping does not provide a usable pulse over the entire depth range.

3) *Negative Residual:* The negative residual portion of the strip signal is a long duration pulse that can be filtered with a long time constant to reduce noise. Using this pulse provides a good signal to noise ratio over much of the depth range but is unusable for interactions near the cathode. This signal changes significantly over depth and would require handling a large dynamic range.

4) *Combined Approach:* A more complex scheme involving two different shaping paths and independently measuring both the positive peak and the residual level may be required to provide the best overall sensitivity. This combination, together with the pixel row pulse height measurement could also be used to provide a measurement of the *Z* coordinate.

Z-dimension measurement: We are pursuing approaches for measuring the *Z* location of interactions without using a signal from the cathode signal. An earlier paper presented a concept and first measurements employing a time-over-threshold circuit on the leading positive lobe of the strip signal to measure *Z* [3]. Another option is to sum all anode signals, strips and pixels. This summed signal would be equivalent to, albeit noisier than, the cathode signal.

IV. SIMULATION & PERFORMANCE OPTIMIZATION

We now present results of recent simulations conducted to help optimize our detector design and operating conditions. A first set of simulations was made in order to predict the response of a 1 cm thick detector using our original anode geometry (Figure 1) and to establish its optimum operations conditions. A second round of simulations was also conducted in an effort to further optimize the anode pattern.

For a given geometry, the electric potential map and the weighting potential maps are first calculated using a commercial 3-d Poisson solver [5]. For an interaction occurring at a given location in the detector, the main electron trajectory is obtained by following the electric field line until the anode face is reached. The electrons are transported along that path considering trapping and detrapping on a shallow trap plus deep trapping. The signals of the various electrodes are then calculated using the relevant weighting potential maps.

These simulations indicate that the 10 mm thick detector will exhibit performances similar to the 5 mm device. Similar energy and position resolutions are expected. Improved efficiencies at higher energies will be achieved with a thicker detector. On the other hand, longer drift lengths might require higher fields for optimum resolution. Also, the *Y* position resolution will remain relatively poorer than in the *X* direction, as was the case for the 5 mm device. Measurements should soon confirm these simulation results.
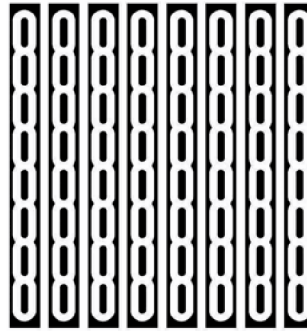

Figure 7. Alternative anode pattern under study with simulation tools.

A second set of simulations was also conducted with different electrode geometries with the aim of improving the *Y* resolution and achieving optimum energy resolution at lower bias. Figure 7 shows what is believed to be an improved electrode pattern. That design retains the pixel-within-strip concept with the same 1 x 1 mm^2 unit cell but the pixels are now elongated in the *Y* direction. This will increase signal sharing between adjacent pixel rows to improve the interpolation algorithm. Also, with larger pixels, compensation between electron trapping and pixel weighting potential drop will occur at lower bias, thus achieving optimum energy resolution at lower bias. To illustrate the compensation, Figure 8 shows simulated signals for interactions occurring at five different depths in the 10 mm device under a bias of 2000 Volts. Events occurring farther from the cathode exhibit longer drift times and thus, due to electron trapping, fewer electrons are collected by the pixel. But these electrons have induced a current in the pixel for a longer period of time and the actual induced charge may be independent of the depth of interaction if the appropriate value of the bias is used.
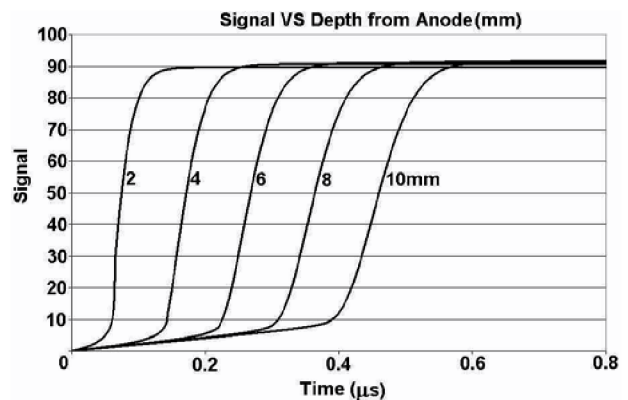

Figure 8. Simulated pixel row signals for interactions at various depths in a 10 mm thick device.

Simulated scans in the *X* and *Y* directions indicate (see Figure 9) that signals induced on neighboring electrodes will provide adequate position information. In particular, the *Y* position resolution should be much improved compared to the previous anode pattern.

To validate these simulations, a new 1 cm thick detector with this new anode geometry will be procured and characterized.
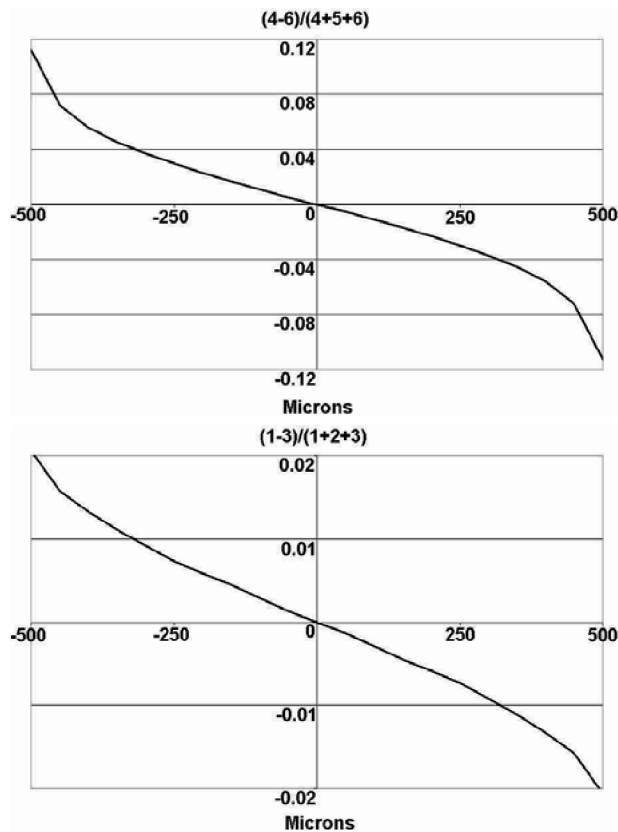
(4-6)/(4+5+6)

(1-3)/(1+2+3)

Figure 9. Top: Signal sharing simulation for strips (*X*-dimension). Bottom: Signal sharing simulation for pixel rows (*Y*-dimension).

V. CONCLUSIONS AND FUTURE WORK

We have made good progress toward our goal of developing and demonstrating a manufacturable design for a compact CZT detector module and image plane qualified for space flight and well suited for a variety of applications.

CZT strip detectors with orthogonal coplanar anodes efficiently detect and locate interactions throughout their volume with good energy resolution and sub-millimeter spatial resolution. This has been demonstrated with 5 mm thick prototype detectors and simulated for 10 mm thick detectors.

We have used simulations and laboratory measurements to study the characteristics of the induced charge signals from the non-collecting anode strips and identified candidate approaches for analog circuits to process these signals for measurement of the *X* and *Z* coordinates of the interactions. Collimated beam spot scans were performed to test a prototype strip signal circuit with 200 ns shaping time. We have demonstrated 0.5 mm position resolution in *X* at 122 keV and estimate reliable 1.0 mm performance is achievable down to 60 keV or lower.

Simulations tools have been developed, validated and employed to explore anode contact options and define optimum geometries and operating conditions for various applications. Simulations of a 10 mm tick device with the same anode

pattern as was previously employed suggest that the thicker device should have signal characteristics similar to the 5 mm device. One option for an alternate anode pattern was presented that will increase the signal sharing between adjacent pixel rows. This is expected to improve the position resolution in the Y-dimension. At the same time, this should allow optimum energy resolution at a somewhat lower bias due to the compensation between the effects of electron trapping and pixel weighting potential.

Future work will include more thorough beam spot mapping and performance evaluation of the existing and new prototype detectors as well as evaluation of prototype circuitry for measurement of energy, *X, Y* and *Z*. Studies of the relative performance of available CZT materials and processes will be conducted.

VI. ACKNOWLEDGEMENTS

VII. REFERENCES

[1] M. L. McConnell, J. R. Macri, J. M. Ryan, K. Larson, L.-A. Hamel, G. Bernard, C. Pomerleau, O. Tousignant, J.-C. Leroux, V. Jordanov, *Three-dimensional imaging and detection efficiency performance of orthogonal coplanar CZT strip detectors*, Proc. SPIE, 4141, 157 (2000).

[2] V.T. Jordanov, J.R. Macri, J.E. Clayton and K.A. Larson, *Multi-Electrode CZT Detector Pacakaging Using Ploymer Flip Chip Bonding,* NIM A 458, 511 (2001).

[3] K. Larson, V. Jordanov, M. L. McConnell, J. R. Macri, J. M. Ryan, A. Drake, L. A. Hamel, O. Tousignant, *Analog processing of signals from a CZT strip detector with orthogonal coplanar anodes,* Proc. SPIE, 4141, 336 (2000).

[4] S. D. Kravis, T. O. Tümer, G. Visser, D. G. Maeding, S. Yin, *Readout Electronics for Nuclear Applications (RENA) IC*, Proc. SPIE, 3445, 364 (1998).

[5] *Coulomb*, by Integrated Engineering Software.